ELSEVIER

Biophysical Chemistry 109 (2004) 137–148

Biophysical Chemistry

www.elsevier.com/locate/bpc

The mechanism of the type III antifreeze protein action: a computational study

Cheng Yang, Kim A. Sharp*

The Johnson Research Foundation, Department of Biochemistry and Biophysics, University of Pennsylvania, Philadelphia, PA 19104, USA

Received 2 September 2003; received in revised form 17 October 2003; accepted 18 October 2003

Abstract

The random network model of water quantitatively describes the different hydration heat capacities of polar and apolar solutes in terms of differential distortions of the water–water hydrogen bonding angle in the first hydration shell. This method of hydration analysis is applied here to study the hydration of the wild type III thermal hysteresis protein from eel pout and three mutations at residue 16. Wild type and one mutant have full activity, the other two mutants have little or no anti-freeze (thermal hysteresis) activity. The analysis reveals significant differences in the hydration structure of the ice-binding site (centered on residue 16) among four proteins. For the A16T and A16Y mutants with reduced activity, polar groups have a typical polar-like hydration. For the wild type and mutant A16C with 100% of the wild type activity, polar groups have unusual, very apolar-like hydration. In the latter case, hydrating water molecules form a more ice-like pattern of hydrogen bonding on the ice-binding face, while in the former case water–water H-bonds are more distorted and more heterogenous. Overall, the binding surface of active protein strongly enhances the water tetrahedral structure, i.e. promotes ice-like hydration. It is concluded that the specific shape, residue size and clustering of both polar/apolar groups are essential for the binding surface to recognize, and preferentially interact with nascent ice crystals forming in liquid water.

Keywords: Antifreeze protein; Thermal hysteresis; Hydration

1. Introduction

Antifreeze or thermal hysteresis proteins (THP) have been found in a variety of organisms, including fish, spiders, insects and bacteria. These proteins are able to depress the freezing point of aqueous solutions by adsorbing to the ice crystal and inhibiting its growth in solution. THPs lower the freezing point of a solution without changing the melting point. The difference between the freezing and the melting point is termed thermal hysteresis, which is widely used as an indicator of THP activity. Several type III THPs' structures have been solved by X-ray [1,2] and NMR technique [3]. Type III THP is a globular protein that consists mainly of β-strands connected by large loops. Its ice-binding face has been studied [4–6] and is distinguished by the relative planarity [2] and apolar character [2,3,5,6]. However, the pre-

*Corresponding author. Tel.: +1-215-573-3506; fax: +1-215-898-4217.

E-mail address: sharpk@mail.med.upenn.edu (K.A. Sharp).

0301-4622/04/$ - see front matter © 2003 Elsevier B.V. All rights reserved.
doi:10.1016/j.bpc.2003.10.024

cise mechanism by which THPs bind to ice crystal and inhibit ice growth is still unclear. Many questions remain regarding the mechanism of specificity and affinity in these proteins. This include the question of how either of THPs' polar or apolar groups can recognize the ice crystals forming in liquid water and how water molecules aggregate on the protein surface. If the protein uses polar groups then ordinarily such groups, being polar, will have a high affinity for liquid water which is present at large excess (55 M), and net binding to ice, present initially at low concentrations, will be negligible. On the other hand, if the protein uses apolar groups, these normally prefer more ice-like water in their hydration shell, but because of their hydrophobicity, their affinity for any kind of water, liquid or ice, will be low. This creates an apparent affinity/specificity dilemma in terms of choosing groups to construct a specific ice nucleus binding surface.

No general mechanism has been proposed by which all antifreeze proteins associate with ice crystal and stop its growth. Three models have been proposed for type I α-helical antifreeze protein. The first is based on a lattice match of the ice oxygen atoms with hydrogen-bonding groups on the protein [7–13]. In contrast, the second model emphasized the role of the hydrophobic part of the amphiphilic helix of the type I THPs in binding to ice surface [14–17]. The third model, a dynamic version of the first model, emphasizes the effect of the initial association of one repeat unit of the helix with ice crystal on the subsequent binding of other repeat units through 'remodeling' of the ice surface [18]. Moreover, none of these models may apply to type III THPs because they lack many structural features of type I THPs, notably the 11-residue Thr-repeat structural motif and their amphiphilic helix. In order to explain type III THP's activity, a model based on alignment of five hydrogen-bonding atoms on the putative ice-binding face and ice oxygen atoms on the prism plane was proposed [1,4]. A subsequent study indicated that side chain orientation and tight packing limit the formation of possible hydrogen bonds and concluded that hydrophobic groups on the ice-binding site might play an important role in the protein–ice interaction [3]. A computer simulation also emphasized the necessity for a favorable orientation that maximizes the hydrogen bond and van der Waals interactions [19]. A neural network study, based on the calculation of contributions from the accessible surface area of the protein, as well as hydrophobic, polar and charged residues, predicted that a certain level of hydrophobicity in the binding site is essential for type III THP's activity [20]. Recent studies found a contribution to THP's activity from hydrophobic residues on the periphery of the putative ice-binding site [5,6].

Previously, we developed a quantitative analysis of changes in water structure induced by polar and apolar solutes based on the random network model (RNM) [25], which characterizes changes in the water–water angle distribution function ($P(\theta)$) [21–24]. The main features of solute induced water structure revealed by this analysis are: the pure water–water angular distribution function ($P(\theta)$) is bimodal with a low-angle population and a high-angle population, centered at approximately 12° and approximately 54°, respectively. Solutes perturb the structure of water principally in their first hydration shell by changing the ratio of these two populations, apolar solutes increasing the low-angle population, polar solutes increasing the high-angle population. There is a direct link between these angular structural changes in the water hydrogen bond network in the first hydration shell of the solute and heat capacity changes. A combination of explicit water simulations and this RNM analysis yields a quantitative agreement between measured and calculated hydration heat capacities, as well as a revealing description of the change in water structure induced by apolar and polar solutes.

Using the water–water angle distribution function ($P(\theta)$), Gallagher and Sharp [26] investigated the hydration structure of type III THP wild type over the entire protein surface, the ice-binding face and the center of the ice-binding face around the key residue ALA 16. This analysis revealed significant differences in the hydration structure of the ice-binding face compared to the non-ice-binding protein surface and non-THP of similar size and structure. In order to better understand the function of type III THP, we further apply this

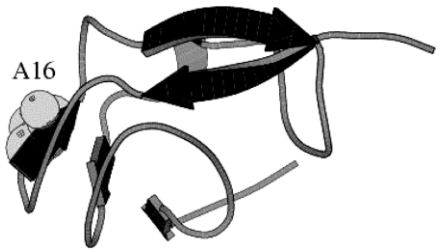

Fig. 1. The crystal structure of type III THP (PDB entry: 1MSI). The key residue ALA 16 in the center of the ice-binding site is in CPK representation.

analysis to study the hydration structure of three type III THPs with residue replacements at position 16. Two specific questions we address are: (i) whether there are significant differences between the hydration structures of the ice-binding site of the wild type and the three mutants, (ii) whether this analysis can shed light on the mechanism of type III THP activity.

2. Methods

2.1. Molecular dynamics simulations

The wild type and three mutants of type III THPs were selected due to their different thermal hysteresis activity and availability of high resolution structures. Mutants A16C, A16T and A16Y have 100, 75 and 33% of wild type, respectively [28]. Their starting coordinates were taken from the Protein Data Bank (PDB entry 1MSI for wild type, 5MSI for A16C, 4MSI for A16T and 7MSI for A16Y). The wild type structure is shown in Fig. 1. CHARMM was used to build the hydrogen atoms needed in the all-atom model. A 63-Å cube of TIP3P water molecule was built using InsightII (Accelerys, San Diego) and equilibrated at 298 K. The water cube was superimposed on the protein structure and overlapping waters were eliminated. The final simulation system consisted of approximately 25 000 atoms including 8002 water molecules, providing at least five layers of solvating water.

All molecular dynamics (MD) simulations were performed using the program CHARMM [27]. For each system, the whole system was first briefly energy-minimized (200 steps ABNR) and then equilibrated over a period of 50 ps. Finally, a 1 ns MD trajectory was generated. The equilibration and trajectory generation were performed by MD using the leapfrog algorithm with a time step of 1 fs, at a constant temperature of 300 K and constant pressure of 1 atm. The Nose–Hoover method was used to maintain constant temperature and the Langevin piston method for constant pressure. Minimum image periodic boundary conditions were employed. In all computations SHAKE constraints were used to fix lengths of bonds involving hydrogen atoms. Electrostatic and van der Waals interactions were truncated using a shifting function between 10.0 and 12.0 Å. Since 1MSI and the mutants are not highly charged proteins, having only eight charged residues—four negative, four positive—for a net charge of 0 at pH 7, it was not necessary to include counterions. These are usually necessary only for highly charged molecules to maintain stable trajectories. For similar considerations we used a cut-off method to handle long-range electrostatics, rather than particle mesh ewald (PME). PME is primarily useful for treating long-range electrostatics in more highly charged systems but has been shown to introduce artifacts in solvent structure. The cut-off method is simpler for low-charge or neutral systems, and been validated by numerous labs working on different proteins. Moreover, the TIP3P water model was parameterized with cut-off method simulations.

2.2. Water–water angular distribution function

The first hydration shell waters were identified by finding all waters within the first hydration shell cut-off of any protein atom. The first shell hydration cut-off for each atom type is defined as the first minimum in the atom–water radial distribution function $g(r)$. The $g(r)$ for each atom type was obtained from preliminary simulations on the model compounds alanine dipeptide and cysteine that contain all the required atom types. Every pair of waters within a water–water distance cut-off was then analyzed, the distance and angle being defined as in Fig. 2. We use here water–water angular distribution function $P(\theta)$ to describe hydrogen bonds within the first hydration shell.

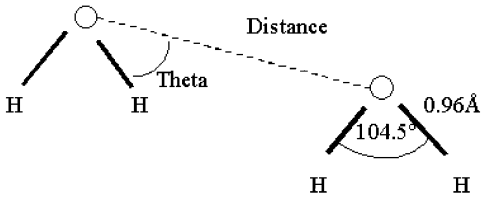

Fig. 2. Water structure. The geometry of the TIP3P water is shown. The water–water angle θ is defined as the minimum of the four HO–O angles. Note that given the TIP3P HOH angle of 104.5°, the maximum possible value of θ is 180° − (104.5°)/2 = 127.8°.

The water–water distance cut-off of 4.0 Å was employed due to its sensitivity in discriminating between hydration heat capacity of polar and apolar solute atoms. We have previously shown [26] that the effects of the protein on the $P(\theta)$ distribution are on the first shell–first shell water geometry. We have monitored all the other pair geometries: first–second, second–second and second–bulk, etc. and have found no statistically significant changes.

For the protein hydration, the water–water angular distribution analysis was carried out using the program PRAM, which uses the CHARMM trajectory files as input. All atoms in the protein are first classified as being apolar, polar or weakly polar, based on the partial charge assigned by the MD force field. Those atoms possessing a charge magnitude less than 0.35 are considered apolar, charge magnitude 0.35–0.45 are classified as weakly polar, and atoms with a partial charge magnitude greater than 0.45 are considered polar. Solute atoms of interest can also be 'tagged' before analyzing the trajectory, allowing the hydration structure of subsets of the protein surface to be examined. Water–water angular distributions are also accumulated separately for the three possible types of solute atom polarity class: polar–polar, apolar–apolar and polar–apolar (mixed). For example, if the first water oxygen was closest to an apolar solute atom and the second water oxygen was closest to a polar solute atom, that water–water angle would be added to the mixed angle frequency histogram.

2.3. Analysis of angle probability distributions

In order to obtain a quantitative comparison of $P(\theta)$ curves the area under each peak, corresponding to the populations of low-angle and high-angle water–water geometry (low angle, denoted A1, high angles, denoted A2), is obtained by numerical integration using the trapezoidal rule as implemented in ORIGIN 6.0. The ratio of these two peak areas A1/A2 is characteristic of the type of solute (apolar, polar, etc.). Reference ratios were calculated from simulations of several small molecules of differing polarity studied previously by Madan and Sharp using the RNM-explicit water method [21,22]. Thus, we may interpret the distribution of water–water angles surrounding the protein surface in relation to small test solutes.

2.4. Surface subsets and controls

The hydration structures of the entire type III THP protein surfaces were evaluated according to the procedures outlined above. We also examined several subsets of the protein surfaces. These included the ice-binding site that is composed of residues 9, 15–18 and 44. We also analyzed the hydration structure surrounding the residue 16 that defines the center of the ice-binding site.

3. Results

The convergence of the simulations was monitored by plotting the root mean squared (rms) deviation of atomic coordinates from the crystal structure as a function of simulation time (Fig. 3). For all four proteins, the results show stable well-converged simulations throughout the 1 ns trajectory, with modest deviations from the crystal structure expected from native state protein fluctuations.

3.1. Overall $P(\theta)$ distributions for type III THPs

The water–water angle distributions for the entire first hydration shell of type III THPs are shown in Fig. 4, and are typical of the profiles seen for the different classes of solvating water pairs seen previously. The apolar–apolar pairs have

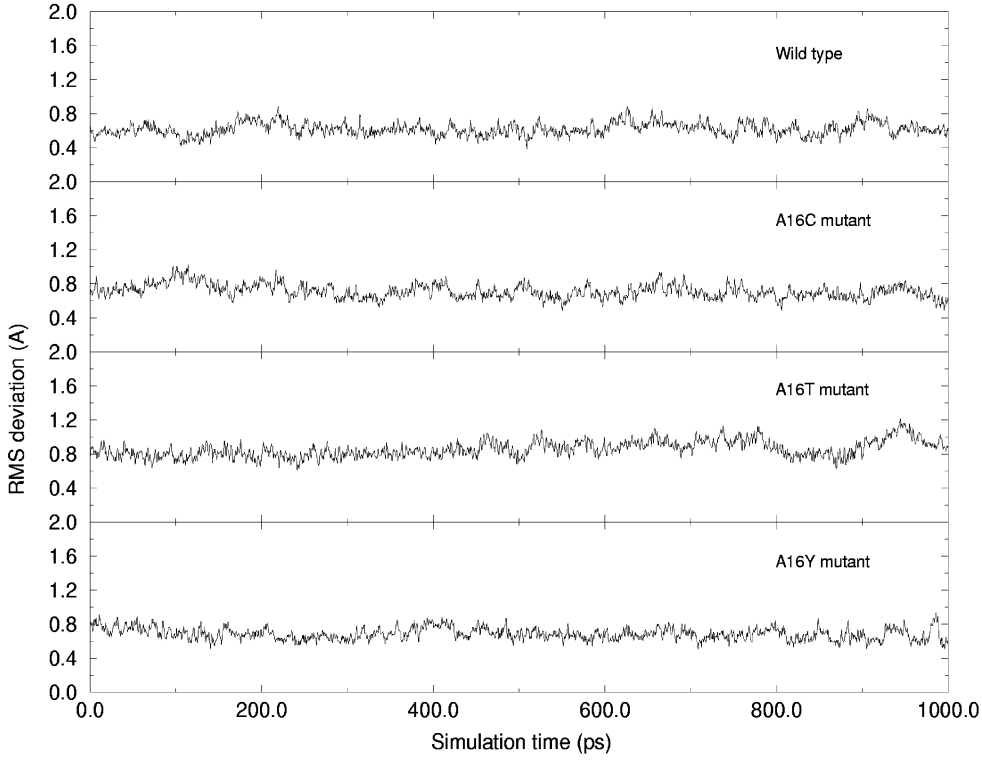

Fig. 3. Simulation convergence behavior, plotted as root mean square deviation in atomic coordinates from the starting crystal structures as a function of simulation time.

a higher fraction of the low-angle population, the polar–polar pairs a higher fraction of the high-angle population. The water–water angle distribution for pure water is used for comparison. Population ratios A1/A2 are summarized in Fig. 7. The characteristic small molecules (methane, potassium, pure water) are included as points of reference and are indicated by the horizontal lines on the histograms. In general, overall water–water angle distributions for the wild type and three mutant proteins are very similar. Thus, the overall water structure around four proteins is similar.

3.2. $P(\theta)$ distributions for type III THP ice-binding sites

The putative type III THP ice-binding site is composed of residues 9, 15–18 and 44. The $P(\theta)$ distributions for wild type and three mutants are shown in Fig. 5. Their population ratios A1/A2 are summarized in Fig. 7. Two main features are noted for the hydration of type III THPs' ice-binding surface, compared to the overall hydration of type III THPs. First, the polar and apolar groups on the ice-binding face both have larger population ratios than that for the entire protein surface. This is true for wild type and three mutants, which demonstrates the ice-binding surface more hydrophobic on average. For the wild type, the A1/A2 ratio for the apolar group on the ice-binding site is 16% larger than the entire protein surface (0.89).

Second, in the ice-binding surface there is now almost no distinction between the apolar and polar water pair angle distributions, in contrast to the entire protein hydration shell. This difference comes primarily from a shift in the angular distributions of polar water-pair towards the apolar-type distribution around the ice-binding site, indicating two things: (i) a less distorted, more tetrahedral

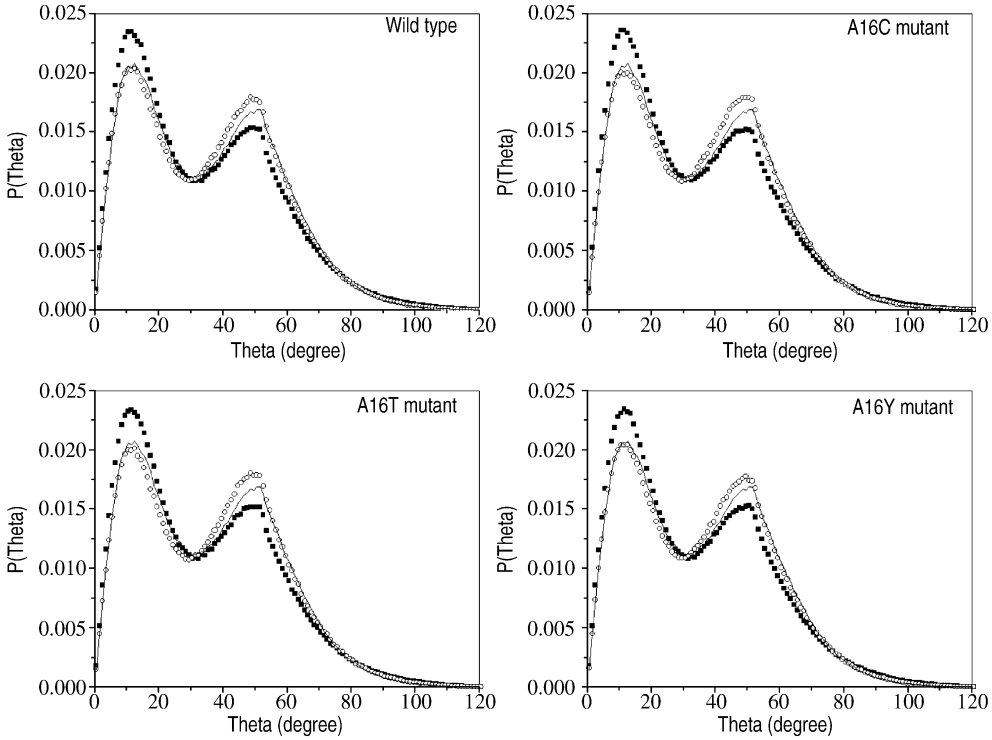

Fig. 4. Overall water structure around type III THPs. The water–water angle probability distributions for the first hydration shell of wild type and three mutant proteins. Hydrating water–water class: (■) apolar, (○) polar, (-) pure water.

or hydrophobic-like water structuring around the ice-binding site; (ii) a more homogeneous, or regular hydration structure around the ice-binding site, i.e. less distinction between polar and apolar group hydration. These changes are apparent in the population ratios in Fig. 7, where the significant change for the ice-binding site is in the A1/A2 ratio for the polar groups. For the wild type, at 0.91 it is approximately 28% greater than that for polar groups on the entire protein surface (0.71). Again the water–water angle distributions for wild type and three mutants show similar shape, indicating similar water structure around their ice-binding sites.

3.3. Water structure around type III THP ice-binding site centers

In order to explain the mechanism of type III THP's activity, hydration in the immediate vicinity of the key residue 16 in the ice-binding site center was further analyzed in the wild type and three mutant proteins. Their $P(\theta)$ distributions are shown in Fig. 6, and their population ratios are summarized in Fig. 7. The most striking feature is that the fraction of the low-angle population around polar groups in the ice-binding site center is *larger* than that around apolar groups for the wild type and active A16C mutant. The large shift to low angles in their $P(\theta)$ distributions for the polar hydrating water class indicates a significant increase in more tetrahedral-like water structure. The water hydrating polar groups around the ice-binding site centers thus has a very apolar-like population ratio. This means that there is uniform hydration structure across the polar and apolar groups in the center of the ice-binding surface of wild type and A16C mutant. In the A16T and A16Y mutants with reduced activities display the standard water structure around the apolar and

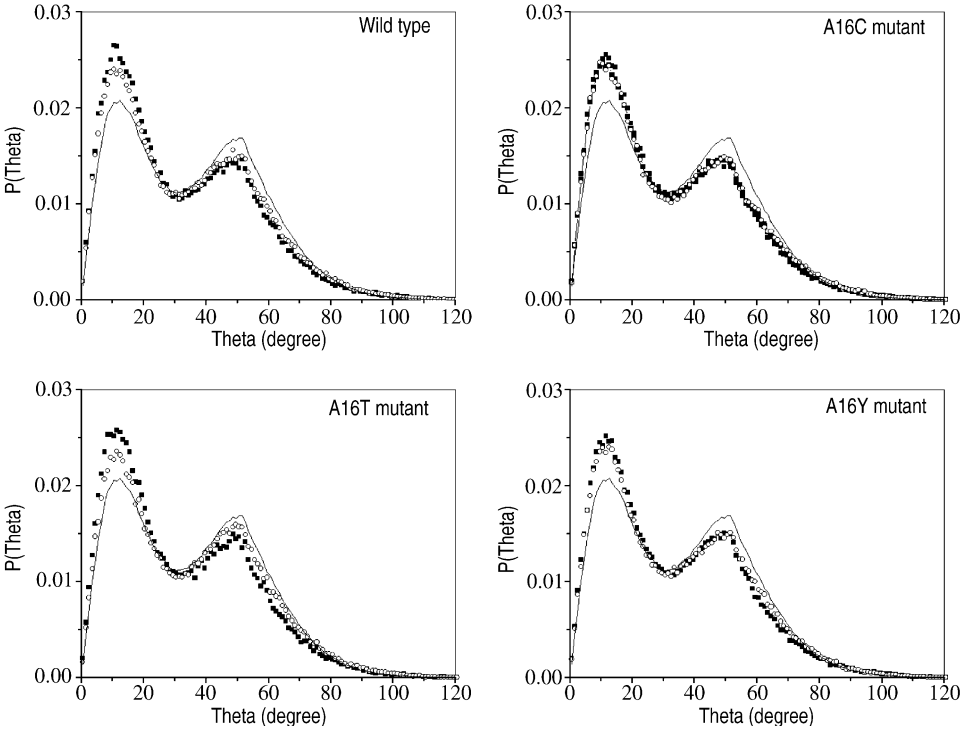

Fig. 5. Water structure around type III THPs' ice-binding sites. The water–water angle probability distributions for the first hydration shell of type III THPs' ice-binding site. Hydrating water–water class: (■) apolar, (○) polar, (-) pure water.

polar groups in the ice-binding site center. This difference indicates that there is some relationship between hydration structure around ice-binding site center and thermal hysteresis activity.

Sample hydration structures around polar groups in the ice-binding site centers are shown in Fig. 8 for the wild type and three mutant, to illustrate the overall shape of the binding surface, the number of waters involved in hydrating residue 16, and a representative hydration configuration. The snapshots were taken from the latter part of the 1 ns trajectories. Polar atoms (O and N with significant negative partial atomic charge) surrounding the center of ice-binding site center are represented in dark colored CPK, residue 16 are represented in light CPK. The water structures in wild type and A16C mutant are quite different from A16T and A16Y mutants. For wild type, hydration structure shows a flat hydrogen bond network between water molecules organizing on the protein surface (black CPK surface), shown in Fig. 8A. Hydrating water molecules interact with seven polar atoms on protein surface (dark CPK coloring), including backbone (14O, 16O, 16N, 17O, 42N) and side chain (18OG1 and 44OE1). Most of these polar atoms have been hypothesized to form hydrogen bonds with water molecules on the ice surface [1,4]. For the A16C mutant, two water–water hydrogen bond network patches are seen around residue 16, shown in Fig. 8B. Three water molecules form a flat hydrogen bond network on the left, others demonstrate a different hydrogen bond plane on the right. Hydrating water molecules solvate seven polar atoms on protein surface, including backbone (14O, 16N, 16O, 17O, 18N) and side chain (42OG and 44NE2). The protein polar atoms and the hydrating water cap form a rather complementary set of H-bonding interactions. In the case of A16T and A16Y mutants, however, water molecules are more unevenly dis-

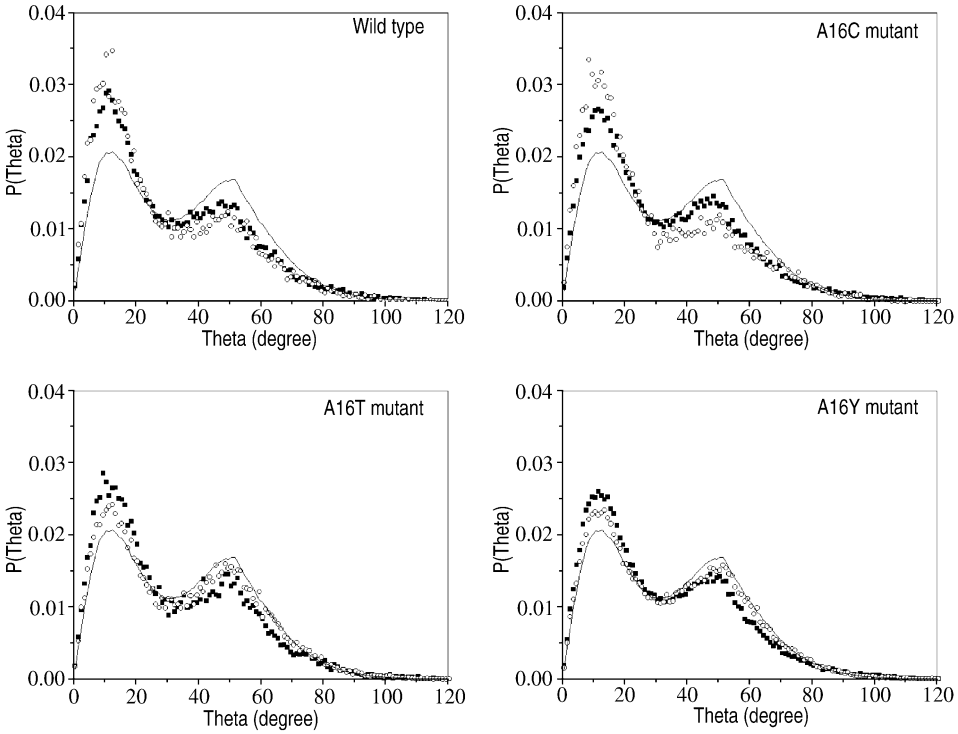

Fig. 6. Water structure around type III THPs' ice-binding site centers. The water–water probability distributions for the first hydration shell of type III THPs' ice-binding site center. Hydrating water–water class: (■) apolar, (○) polar, (-) pure water.

tributed around residue 16, as shown in Fig. 8C and D. Examination of these and several other snapshots shows that it is less common to see a specific complementary arrangement between water molecules and the indicated polar atoms in large part due to steric interference from the larger T16 and Y16 side chains.

4. Discussion

This work was motivated by the ability of the RNM analysis of water hydration to reveal subtle but important changes in water structure induced by the polar and apolar solutes [21–24,26], and by the desire to better understand the mechanism of type III THP's activity. We have performed extended MD simulations of type III antifreeze wild type protein and three mutants in water using the CHARMM/TIP3P potential functions and analyzed their hydration structures. A newly developed software program, PRAM, was then be used to calculate the distribution of water–water angles, $P(\theta)$ for the protein hydration shell. Numerical integration of the two peaks in the $P(\theta)$ distribution and calculation of the low- to high-angle population ratio (A1/A2) was used as a quantitative method to analyze changes in $P(\theta)$. This value can be easily computed for the entire protein surface or for any part of it, and the results interpreted using values obtained from small solutes as a reference. Furthermore, the A1/A2 ratio defines the populations in relation to pure water and reference values for hydration of apolar/polar small molecules provide us with a quantitative measure of changes in hydrating water structure around different protein groups.

Applying this analysis to type III THP wild type and three mutant proteins, we can draw several conclusions. First, we note that the relative overall population ratios for apolar and polar hydrating

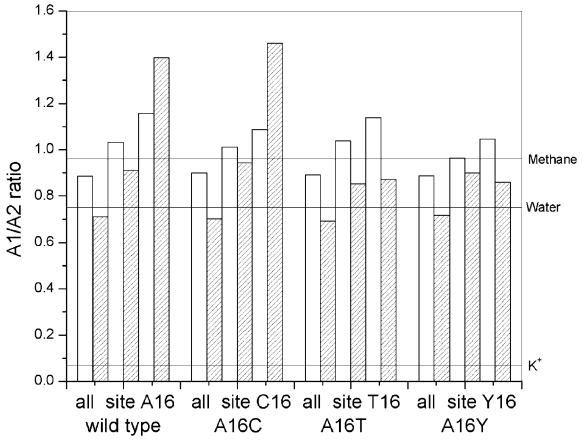

Fig. 7. Summary of $P(\theta)$ population ratios. The ratio of low-angle to high-angle populations in the water–water angle probability distributions for the entire protein surface (all), the ice-binding site (site) and the ice-binding site center. Unshaded bars, shaded bars indicate apolar and polar hydrating water–water classes, respectively. Ratios for pure water, and for hydration of methane and potassium are shown as horizontal lines for reference.

water pairs follow the expected trend based on polarity, and are similar for four proteins. These ratios may be interpreted as a reflection of the overall hydrophobicity of protein surface. Second, the differences between polar and apolar protein group hydration are much smaller than the range seen in small molecule hydration. For example, compared to our small standard molecule (K^+), the polar protein atoms' $P(\theta)$ distributions are not as distorted, indicating that either water has a relatively weak interaction with these groups or the effect of neighboring polar and apolar groups on the surface tend to cancel. When we examine the ice-binding surfaces of these four proteins, significant differences between ice-binding regions and entire proteins emerges. First, the hydration structure of the polar atoms in ice-binding sites contains a greater amount of tetrahedral structure or ice-like water structure. The apolar groups in the functional patch also exhibit more hydrophobic-like hydration, with even greater A1/A2 ratios than the hydrophobic reference (methane). Second, the hydration structure is more uniform over the ice-binding site, i.e. there is less variation between the polar and apolar hydration. However, looking at the whole ice-binding sites, we cannot find much difference in the overall ice-binding surface hydration among wild type and three mutants although these four proteins have different thermal hysteresis activities.

However, if we further narrow our focus to study the structuring of water around the key residue 16 in the center of ice-binding site, we observe even greater differences among different proteins with different activities, primarily with regards to polar atom hydration. For wild type and A16C mutant with 100% activity of wild type, water molecules solvating polar groups in ice-binding site center have structures very uncharacteristic of polar hydration, and it is in fact more ice-like than water molecules hydrating apolar groups. This conclusion is based on analysis of average of many water configuration over an extended simulation. In structural terms, the hydration in the ice-binding center of A16 and A16C THPs can be described qualitatively as follows: there is formation of a water hemisphere or cap with clathrate-like structure over residue 16 which is 'anchored' at its edges by interaction with the immediately surrounding polar groups. We interpret this to imply the preference of this subsection of the ice-binding surface, in terms of both affinity and specificity, for more ordered water or ice. The hydration structure around residue 16 also has the effect of making the hydration structure of the ice-binding face in general more uniform across polar and apolar regions. Again, we interpret this effect as strengthening the affinity for ordered water structures and so favoring binding to the more structured ice form of water over the liquid form. The arrangement of ordered water molecules with protein polar atoms forms shape complementary between hydration surface and protein surface, which could enhance affinity to ice water. These polar atoms in the active type III THP ice-binding face, unlike usual polar groups drive water molecules to adopt the water pair conformation with apolar hydration characteristics. This effect is missing in A16T and A16Y mutants with reduced activities: the polar groups in residue 16 show standard polar hydration. These differences clearly indicate that THP activity may require the key

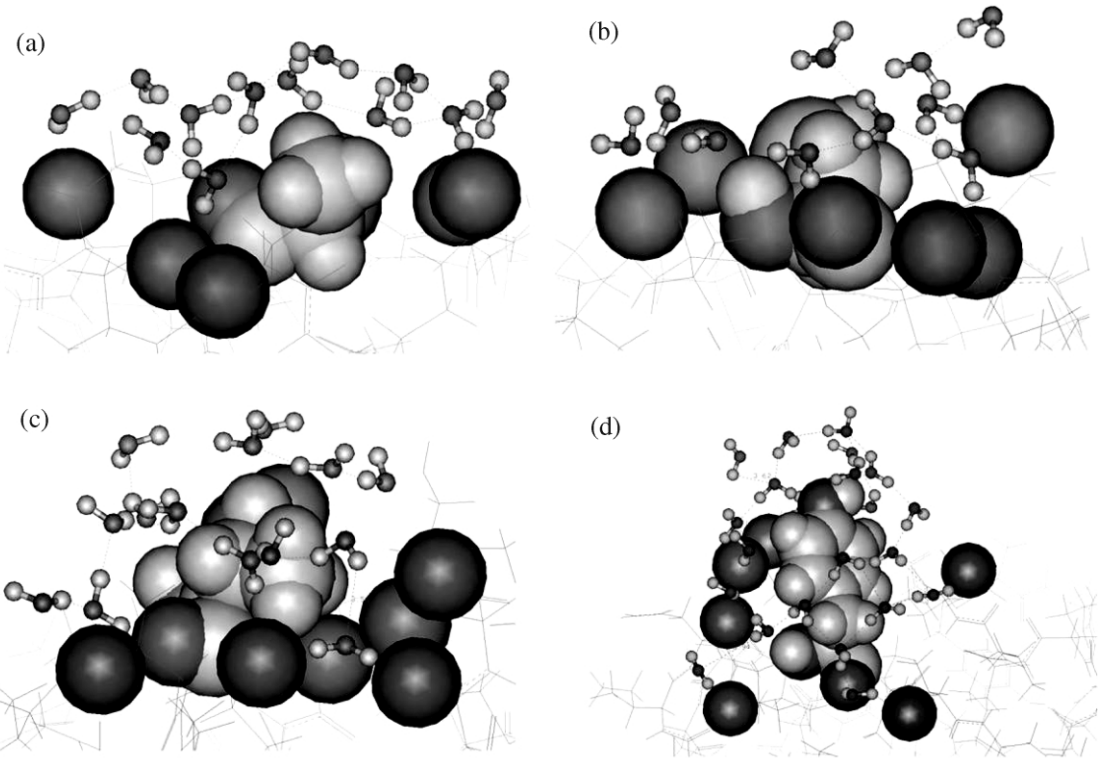

Fig. 8. Water structure around the polar groups in type III THP ice-binding site centers. The snapshots are taken from 1 ns trajectory final structures of wild type and three mutant proteins. Negative partial charge atoms (O, N) are represented by black CPK, the residue 16 atoms in the ice-binding centers are represented by gray CPK. The rest of the protein is shown in wire-frame. Water is shown in ball and stick representation. Proteins: (A) Wild type, (B) A16C, (C) A16T and (D) A16Y.

residue 16 in the ice-binding site to play a dual role—maintain a flat, apolar surface, and along with its neighboring polar groups, to create polar group hydration with apolar structure. Again, these conclusions are based on analysis of the average water structures. The snapshots of solvation structure in Fig. 8 primarily illustrate the overall size, shape and number of waters in the hydration shells, and provide a structural but qualitative rationale for the less regular hydration pattern seen in the inactive mutants.

Regarding the progression of hydration structure shown in Figs. 4–6, which refer to the hydration pattern over the whole protein, the binding face, and the region in the center of binding around residue 16, respectively, we draw two conclusions: First, that the unique hydration pattern in active THPs (polar residue hydration that is more 'ice-like' than that of hydrophobics) is local and specific, confined to the region immediately surrounding the binding site center, located around residue 16. This is shown by the fact that only in Fig. 6 do we see the effect. The local effect is consistent with its origin: a combination of apolar and polar (but net neutral) groups on the protein surface. Thus, the effect is partly due to apolar forces (shape, hydrophobicity), and partly electrostatic in nature with dipolar (hence, short ranged) interactions. Second, because the unique hydration pattern in active THPs is local, it explains the experimental observation that a single point mutation can abolish activity. Also, the fact that we see normal hydration over the rest of the protein—which is non-ice-binding—in effect forms a control observation.

We propose that active type III THPs work as follows: upon ice crystals forming in liquid water, polar groups around residue 16 favor binding to this ice over liquid water due to their propensity for flatter, more ordered hydration structure with ice-like water–water angles. In contrast, polar groups around residue 16 of the inactive mutants prefer binding to liquid water (with more distorted structure) which is present in large excess, over ice. Clearly the bulky side chain mutants, such as A16T and A16Y, also lessen the flatness of their ice-binding regions and loss of the protein–ice shape complementary will also be a factor in lowering affinity. This is consistent with the observed highly conserved flatness of ice-binding faces [2,28].

Although there is no generally accepted mechanism by which all THPs act, several hypotheses based on specific type of structural features and surface group properties have been proposed [1,3,4,7–13,16–20,29]. A major argument among these hypotheses is whether THPs bind to the ice surface using polar or apolar groups. The calculations and analysis presented here reveal that the polar groups around apolar residue 16 demonstrate apolar hydration property, implying their propensity for ice-like water structure. This provides a solution to the affinity/specificity dilemma associated with using either polar groups (nominally with high affinity and low specificity) or apolar group (nominally with low affinity and high specificity), and implies that both polar and apolar groups in close proximity are required.

5. Conclusions

MD simulations of type III THP wild type and three mutants in the key residue 16 in the ice-binding face center were performed. The MD trajectories were used to analyze the solute induced distortion of water structure within the framework of the RNM, which quantitatively describes hydrophobic or hydrophilic hydration. The water–water angular distribution function ($P(\theta)$) revealed that the overall hydration structure of four proteins and the hydration structure of their ice-binding site both have standard features, apolar pairs with a higher low-angle population while polar pairs with a lower high-angle population. In contrast, the water–water angular distribution function showed significant differences in the hydration structure at the center of the ice-binding site center among wild type and three mutant THPs with different activities. For wild type and the A16C mutant with 100% of the wild type activity, polar groups in residue 16 have a very apolar-like hydration. For A16T and A16Y mutants with reduced activity, polar groups show standard polar-like hydration. The more ice-like hydrating water structures formed on the ice-binding faces of the active THPs implies that this protein surface has a high affinity and specificity for more ordered or ice-like water, and thus for ice itself. The structure–function relationship suggests that the high affinity of the type III THPs binding for ice nuclei requires dual characteristics of the protein ice-binding surface, i.e. polar groups in proximity to apolar groups, and having apolar-like hydration properties.

Acknowledgments

We thank Dr K.R. Gallagher, Dr N.V. Prabhu and Dr M. Panda for helpful discussions. Financial support is acknowledged from NIH (GM54105).

References

[1] Z. Jia, C.I. DeLuca, H. Chao, P.L. Davies, Structural basis for the binding of a globular antifreeze protein to ice, Nature 384 (1996) 285–288.
[2] D.S. Yang, W.C. Hon, S. Bubanko, et al., Identification of the ice-binding surface on a type III antifreeze protein with a 'flatness function' algorithm, Biophys. J. 74 (1998) 2142–2151.
[3] F.D. Sönnichsen, C.I. DeLuca, P.L. Davies, B.D. Sykes, Refined solution structure of type III antifreeze protein: hydrophobic groups may be involved in the energetics of the protein–ice interaction, Structure 4 (1996) 1325–1337.
[4] H. Chao, F.D. Sönnichsen, C.I. DeLuca, P.L. Davies, B.D. Sykes, Structure–function relationship in the globular type III antifreeze protein: identification of a cluster of surface residues required for binding to ice, Protein Sci. 3 (1994) 1760–1769.
[5] G. Chen, Z. Jia, Ice-binding surface of fish type III antifreeze, Biophys. J. 77 (1999) 1602–1608.
[6] J. Baardsnes, P.L. Davies, Contribution of hydrophobic residues to ice binding by fish type III antifreeze protein, Biochim. Biophys. Acta 1601 (2002) 49–54.

[7] D.S.C. Yang, M. Sax, A. Chakrabartty, C.L. Hew, Crystal structure of an antifreeze polypeptide and its mechanistic implications, Nature 333 (1988) 232–237.
[8] C.A. Knight, C.C. Cheng, A.L. DeVries, Adsorption of alpha-helical antifreeze peptides on specific ice crystal surface planes, Biophys. J. 59 (1991) 409–418.
[9] D. Wen, R.A. Laursen, A model for binding of an antifreeze polypeptide to ice, Biophys. J. 63 (1992) 1659–1662.
[10] D. Wen, R.A. Laursen, Structure–function relationships in an antifreeze polypeptide: the role of neutral, polar amino acids, J. Biol. Chem. 267 (1992) 14102–14108.
[11] D. Wen, R.A. Laursen, A D-antifreeze polypeptide displays the same activity as its natural L-enantiomer, FEBS Lett. 317 (1993) 31–34.
[12] D. Wen, R.A. Laursen, Structure–function relationships in an antifreeze polypeptide: the effect of added bulky groups on activity, J. Biol. Chem. 268 (1993) 16401–16405.
[13] D. Wen, R.A. Laursen, Structure–function relationships in an antifreeze polypeptide: the role of charged amino acids, J. Biol. Chem. 268 (1993) 16396–16400.
[14] S.M. McDonald, A. White, P. Clancy, J.W. Brady, Binding of an antifreeze polypeptide to an ice/water interface via computer simulation, AIChE J. 41 (1995) 959–973.
[15] A. Cheng, K.M. Merz Jr., Ice-binding mechanism of winter flounder antifreeze proteins, Biophys. J. 73 (1997) 2851–2873.
[16] A.D.J. Haymet, L.G. Ward, M.M. Harding, C.A. Knight, Valine substituted winter flounder 'antifreeze': preservation of ice growth hysteresis, FEBS Lett. 430 (1998) 301–306.
[17] A.D.J. Haymet, L.G. Ward, M.M. Harding, Winter flounder 'antifreeze' proteins: synthesis and ice growth inhibition of analogs that probe the relative importance of hydrophobic and hydrogen-bonding interactions, J. Am. Chem. Soc. 121 (1999) 941–948.
[18] M.E. Houston Jr., H. Chao, R.S. Hodges, et al., Binding of an oligopeptide to a specific plane of ice, J. Biol. Chem. 273 (1998) 11714–11718.
[19] J.D. Madura, M.S. Taylor, A. Wierzbicki, J.P. Harrington, C.S. Sikes, F.D. Sönnichsen, The dynamics and binding of a type III antifreeze protein in water and on ice, J. Mol. Struct. 388 (1996) 65–77.
[20] S.P. Graether, C.I. DeLuca, J. Baardsnes, G.A. Hill, P.L. Davies, Z. Jia, Quantitative and qualitative analysis of type III antifreeze protein structure and function, J. Biol. Chem. 274 (1999) 11842–11847.
[21] B. Madan, K. Sharp, Heat capacity changes accompanying hydrophobic and ionic solvation: a Monte Carlo and random network model study, J. Phys. Chem. 100 (1996) 7713–7721.
[22] K.A. Sharp, B. Madan, Hydrophobic effect, water structure, and heat capacity changes, J. Phys. Chem. B 101 (1997) 4343–4348.
[23] F. Vanzi, B. Madan, K. Sharp, Effect of the protein denaturants urea and guanidinium on water structure: a structure and thermodynamic study, J. Am. Chem. Soc. 120 (1998) 10748–10753.
[24] K.R. Gallagher, K. Sharp, A new angle on heat capacity changes in hydrophobic solvation, J. Am. Chem. Soc. 125 (2003) 9853–9860.
[25] A.R. Henn, W. Kauzmann, Equation of state of a random network. Continuum model of liquid water, J. Phys. Chem. 93 (1989) 3770–3783.
[26] K.R. Gallagher, K. Sharp, Analysis of thermal hysteresis protein hydration using the random network model, Biophys. Chem. 105 (2003) 195–209.
[27] B.R. Brooks, R.E. Bruccolcri, B.D. Olafson, D.J. States, S. Swaminathan, M. Karplus, CHARMM: a program for macromolecular energy minimization and dynamics calculations, J. Comp. Chem. 4 (1983) 187.
[28] C.I. DeLuca, P.L. Davies, Q. Ye, Z. Jia, The effects of steric mutations on the structure of type III antifreeze protein and its interaction with ice, J. Mol. Biol. 275 (1998) 515–525.
[29] J.D. Madura, K. Baren, A. Wierzbicki, Molecular recognition and binding of thermal hysteresis proteins to ice, J. Mol. Recognit. 13 (2000) 101–113.